ISSN 0915-633X

NATIONAL INSTITUTE FOR FUSION SCIENCE

Measuring Method of Decay Time of Negative Muonlike Particle by Beam Collector Applied RF Bias Voltage

J. Uramoto

(Received - Oct. 7, 1997)

NIFS-530 Dec. 1997

RESEARCH REPORT
NIFS Series

NAGOYA, JAPAN

Measuring Method of Decay Time of Negative Muonlike Particle by Beam Collector applied RF Bias Voltage

Jōshin URAMOTO

National Institute for Fusion Science
332-6 Orosh-cho, Toki-shi, Gifu, 509-52, Japan

Abstract

The decay time of negative muonlike particle μ^- is estimated from the final secondary electron current characteristic in the beam collector (BC) of the magnetic mass analyzer (MA) where a radio frequency (RF) bias voltage is applied. The secondary electron current between BC and MA is produced by the final secondary electrons due to μ^- and positive ions in MA, which depends on the RF frequency of the RF bias voltage to BC. When a period of the RF frequency approaches to the decay time of μ^-, the secondary electron current to BC decreases abruptly (e-folding).

Keywords: negative muonlike particle μ^-, μ^- decay time, RF bias voltage

1. Introduction

Usually, it is easy to measure the decay time τ_π of low energy negative pion from a flight distance l_π in free space. Because the typical flight distance under an acceleration voltage V_E (V) is estimated by $l_\pi = v_\pi \tau_\pi \approx 3.9 \times 10^6 \sqrt{V_E}$ (cm/sec) $\times 2.6 \times 10^{-8}$ (sec) $\approx 10^{-1} \sqrt{V_E}$ cm and l_π is about 3.0 cm for $V_E = 800$V in our experiments, (where v_π is a velocity of the pion). On the other hand, it is difficult within a small experimental apparatus to measure the decay time τ_μ of negative muon from a flight distance l_μ in free space. Because the typical flight distance under an acceleration voltage V_E (V) is estimated by $l_\mu = v_\mu \tau_\mu \approx 4.5 \times 10^6 \sqrt{V_E}$ (cm/sec) $\times 2.2 \times 10^{-6}$ (sec) $\approx 10\sqrt{V_E}$ cm and l_μ is above 3×10^2 cm even if $V_E = 800$V. (where v_μ is a velocity of the muon). Thus, in order to measure the decay time of the muon, we must use other measuring methods except the flight distance.

In our experiments as described later[1], a net current of the muonlike particle μ^- is too small (around 0.01 μA) to measure the decay time from the ordinary characteristic X ray. Therefore, we will use the final secondary electrons to measure the decay time τ_μ of μ^- in this paper. That is, the following processes are used:

$$\mu^- \rightarrow e_H + v, \quad \cdots\cdots (1)$$

$$e_H \rightarrow Ne_S, \quad \cdots\cdots (2)$$

where e_H is high energy electron due to the μ^- decay, e_S is the final secondary electron generated inside of the beam collector BC of the mass analyzer, N is number of e_S and v is a neutrino.

As reported already[1], the secondary electrons Ne_S inside of BC induce a greatly increased electron current between BC and MA when a dc positive bias voltage is applied to BC and positive ions exists in front of BC. Then, if a radio frequency (RF) bias voltage is applied to BC instead of the dc bias voltage, the secondary electron current characteristic will depend on the RF frequency through the period.

In this paper, a measuring method of the μ^- decay time will be found from a relation between a characteristic frequency of the applied RF voltage and the μ^- decay time.

2. Pre-experiment (1)

Schematic diagrams of the experimental apparatus are shown in Fig. 1. The apparatus is constructed from a H_2 gas discharge plasma in magnetic fields, three extraction electrodes (with an aperture of 3 mm in diameter) to extract some negatively charged particles and a magnetic mass analyzer (90° deflection-type).

A sheet plasma[2] is produced to generate H^- ions effectively and in wide area. That is, the discharge (cylindrical) plasma flow of about 1 cm in diameter is transformed into a sheet plasma flow of about 3 mm in thickness and about 20 cm in width, while the electron components in the initial discharge plasma are accelerated near 55 eV. The sheet plasma flow enters the electron acceleration anode through the main chamber (50 cm long). A uniform magnetic field of about 50 gauss is applied along the sheet plasma flow in the main chamber where the H_2 gas pressure is about 1.5×10^{-3} Torr. The electron acceleration anode current I_A is 20A. A distance between the sheet plasma center and the first extraction electrode (L) is 7.5 cm. The plasma density in the center of the sheet plasma is about 10^{11}/cc and the electron temperature is about 20 eV. The positive ion density in front of the first extraction electrode is estimated to be about 10^{10}/cc from a positive ion saturation current as H_3^+, while the electron density from the Langmuir probe characteristic is about 10^9/cc and the electron temperature is about 3.0 eV. That is, the electron density in front of the first extraction electrode is reduced near 1/10 of the positive ion density.

The negatively charged particles extracted from the H_2 gas discharge plasma, are injected into the ordinary magnetic mass analyzer (MA) through the slit (3 mm × 1 cm) while each mass of the negatively charged particle is estimated by the following relations: From the analyzing magnetic field B_M where the negative current to the beam collector BC shows a peak, the curvature radius r of the mass analyzer and the extraction (acceleration) voltage V_E, we can estimate the mass m of the negatively charged particle by,

$$m = \frac{Ze\,(B_M r)^2}{2V_E}$$

$$= \frac{8.8 \times 10^{-2}\, Z\,(B_M r)^2\, m_e}{V_E}, \quad \cdots\cdots (1)$$

where e is the electron charge, B_M is in gauss unit, r is in cm unit, V_E is in volt unit and m_e is the electron mass and Z is the charge number. For the curvature radius $r = 4.3$ cm of this mass analyzer, the Eq. (1) is rewritten by

$$m = \frac{1.63\ Z\ B_M^2}{V_E} m_e. \quad \cdots\cdots (2)$$

In the extraction of negatively charged particles, the first extraction electrode (L) is electrically floated, whose potential V_L is about −10V with respect to the electron acceleration anode. A potential V_M of the second extraction electrode (M) is kept at 75V. A potential V_E of the final extraction electrode (E) is 800V.

Thus, as reported in the previous paper[1], the negative muonlike particles are extracted with H^- ions and high energy electrons.

3. Pre-experiment (2)

We have already reported[1] that the charge compensation of the secondary electrons due to decay of the muonlike particle μ^- needs a large charge effect of positive ions, and that the back ground low energy electrons within the mass analyzer MA must be removed by arranging a side metal plate SP as shown in Figs. 2 (A) and (B). The dependences of negative current I^- (to beam collector BC) on the analyzing magnetic field B_M under $V_{BC} = 50$V are shown in Fig. 3 for the two bias voltages V_{SP} of SP. Moreover, the dependences of the peak current I_P^- (corresponding to μ^-) on V_{SP} are shown in Fig. 4 with the negative current I_S^- to SP. Then, it should be noted that the I_P^- saturates above $V_{SP} \approx 100$V. We can consider that the back ground low energy electrons within MA are removed above $V_{SP} = 100$V sufficiently for increment of the positive ion charge effect.

4. Experimental Research for μ^- decay time

As shown in Figs. 5 (A) and (B), a RF bias voltage is applied to the beam collector BC instead of the dc bias voltage. Then, dependences of the negative current I^- (to BC) on the analyzing magnetic field B_M are shown in Fig. 6 for a RF voltage $V_{RF} = 100$V (square wave) at a frequency of RF $f = 1$ kHz under $V_{SP} = 25$V or 100V. A current peak I_P^- of the negative current I^-

(to BC) is seen also near the analyzing magnetic field $B_M \approx 1.3 \times 240$ gauss (corresponding to the μ^- particle). Dependence of the current peak I_P^- on the RF bias voltage V_{RF} under $V_{SP} = 100V$ and RF frequency $f = 1$ kHz is shown in Fig. 7 with a current I_S^- to SP, where I_P^- saturates for $V_{RF} > 90V$. Next, under $V_{RF} = 100V$, their e-folding values of I_P^- are investigated for the RF frequencies as shown in Fig. 8. When the V_{SP} increases, the characteristic frequency for the e-folding value of I_P^- approaches to about $f_C = 450$ kHz. Obviously, we find that the period of f_C (~2.2 μsec) is near the decay time of the typical negative muon (2.22 μsec). It should be noted that the characteristic period of f_C agrees with the typical decay time under the two saturated conditions ($V_{SP} = 100V$ and $V_{RF} = 100V$).

References

1) J. Uramoto: National Institute of Fusion Science, Nagoya, Japan-Research Report, NIFS-(1997).

2) J. Uramoto: Journal of the vacuum society of Japan, **27** (1984) 610.

Figure Captions

Fig. 1 Schematic diagram of experimental apparatus.

1: Cylindrical plasma in discharge anode. 2: Discharge cathode. 3: H_2 gas flow. 4: Discharge power supply. 5: Electron acceleration power supply. 6: Vacuum pump. 7: Area where cylindrical plasma is transformed into sheet plasma. 8: Insulation tube. 9: A pair of permanent magnets. 10: Magnetic field coils. 11: Electron acceleration anode. I_A: Current to electron acceleration anode. CP: Cylindrical plasma. SP: Sheet plasma. B_Z: Magnetic field. L: First extraction electrode. M: Second extraction electrode. E: Final extraction electrode. V_M: Potential (75V) of second extraction electrode with respect to electron acceleration anode. V_E: Potential (800V) of final extraction electrode with respect to electron acceleration anode. MA: Magnetic deflection (90°) mass analyzer. B_M: Magnetic field intensity of MA. BC: Beam collector of MA. V_{BC}: Positive potential of BC with respect to MA. I^-: Negative current to BC. $H\bar{0}$: Hydrogen negative ions outside of sheet plasma. H^-: Accelerated hydrogen negative ions. $\pi\bar{0}$: Negative pionlike particles outside of sheet plasma. μ^-: Accelerated negative muonlike particles.

Figs. 2 (A) and (B) Schematic diagrams of mass analyzer MA under arrangement of side metal plate SP.

S: Entrance slit. X: Entrance of uniform magnetic field (B_M). + Ion: Positive ions in front of BC. Ins: Insulator behind BC. (e_H): High energy electrons. (π^-): Accelerated negative pionlike particles. SP: Side metal plate (1.5 cm × 1.0 cm). V_{SP}: Bias voltage of SP with respect to MA. I_S^-: Negative current to SP. C: Magnetic coil. (N): North pole of electro-magnet. (S): South pole. B_M: Analyzing magnetic field (uniform). Fe: shows Iron.

(See Figure caption of Fig. 1).

Fig. 3 Dependences of negative current I^- (to BC) on B_M for two bias voltages of SP under $V_{BC} = 50V$.

V_{SP} = Bias voltage of SP. (1): $V_{SP} = 25V$. (2): $V_{SP} = 100V$. I_P^-: Current peak corresponding to negative muonlike particle μ^-. I_H^-: Current peak of H^- ion.

Fig. 4 Dependences of I_P^-, I_H^- and I_S^- (to SP) on V_{SP}.

(See Figure caption of Figs. 2 and Fig. 3)

Figs. 5 (A) and (B) Schematic diagrams of mass analyzer MA under RF bias voltage.

RF: RF bias voltage applied to BC.

(See Figure caption of Figs. 2)

Fig. 6 Dependence of negative current I^- (to BC) on B_M under a RF bias voltage V_{RF} = 100V of square wave at frequency f = 1 kHz. (1): V_{SP} = 25V (bias voltage of SP). (2): V_{SP} = 100V. I_P^-: Current peak corresponding to negative muonlike particle μ^-. I_H^-: Current peak of H^- ion.

Fig. 7 Dependence of negative current peak I_P^- on RF bias voltage V_{RF} under V_{SP} = 100V and RF frequency f = 1 kHz.

V_{SP}: Bias voltage of SP. I_S^-: Current to SP.

Fig. 8 Dependences of negative current peak I_P^- on RF frequency f under various bias voltages V_{SP} of SP.

I_P^-: Current peak corresponding to μ^-. I_{P0}^-: I_P^- at f = 1 kHz. RF voltage: V_{RF} = 90V (square wave). f_C: Characteristic frequency where I_{P0}^- decreases 1/2.7

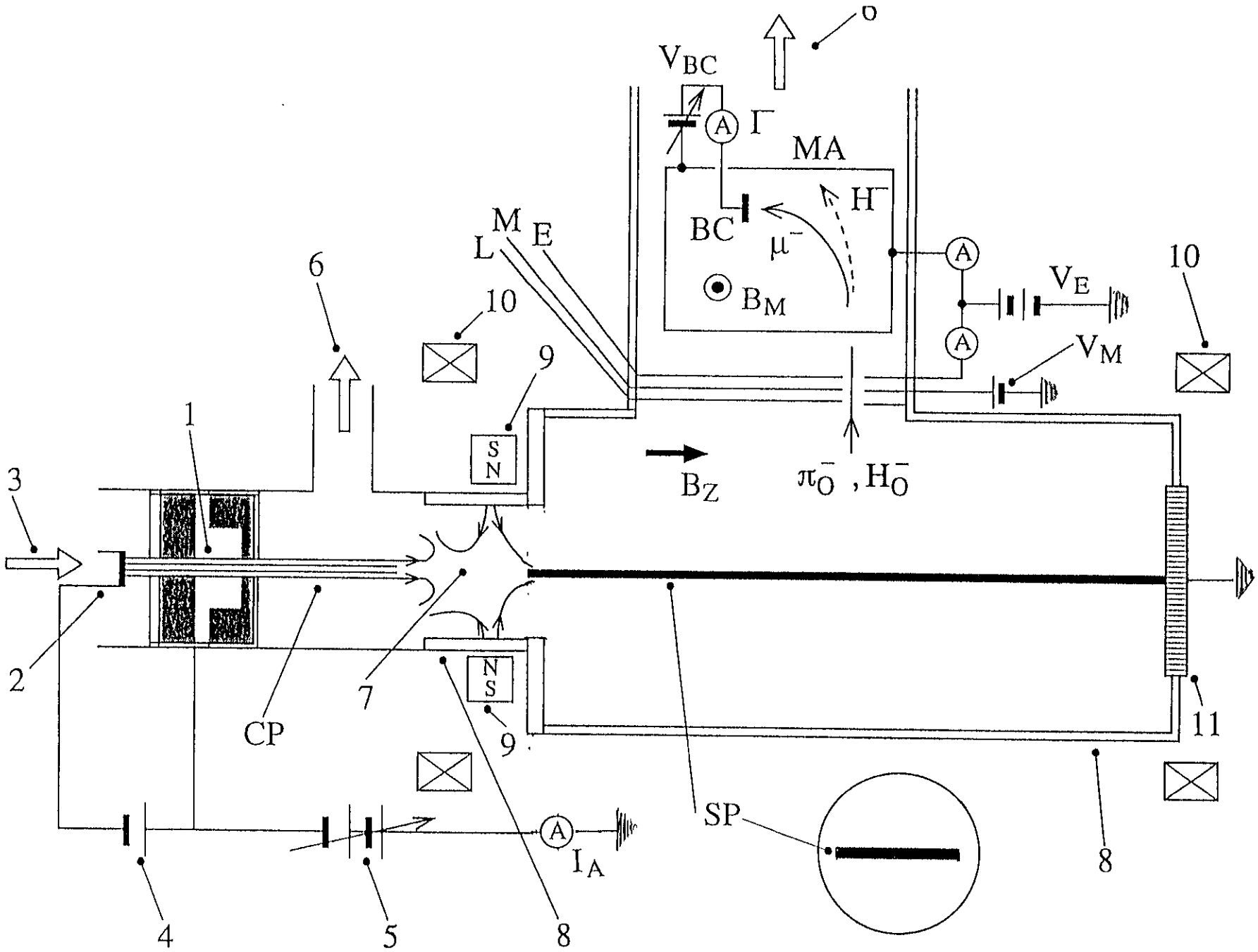
0
V_{BC}
A
Γ
MA
H⁻
BC
μ⁻
B_M
L
M
E
6
10
9
S
N
1
3
2
CP
7
N
S
9
B_Z
π_0^- , H_0^-
A
V_E
A
V_M
10
11
SP
8
A
I_A
4
5
8

Fig. 1

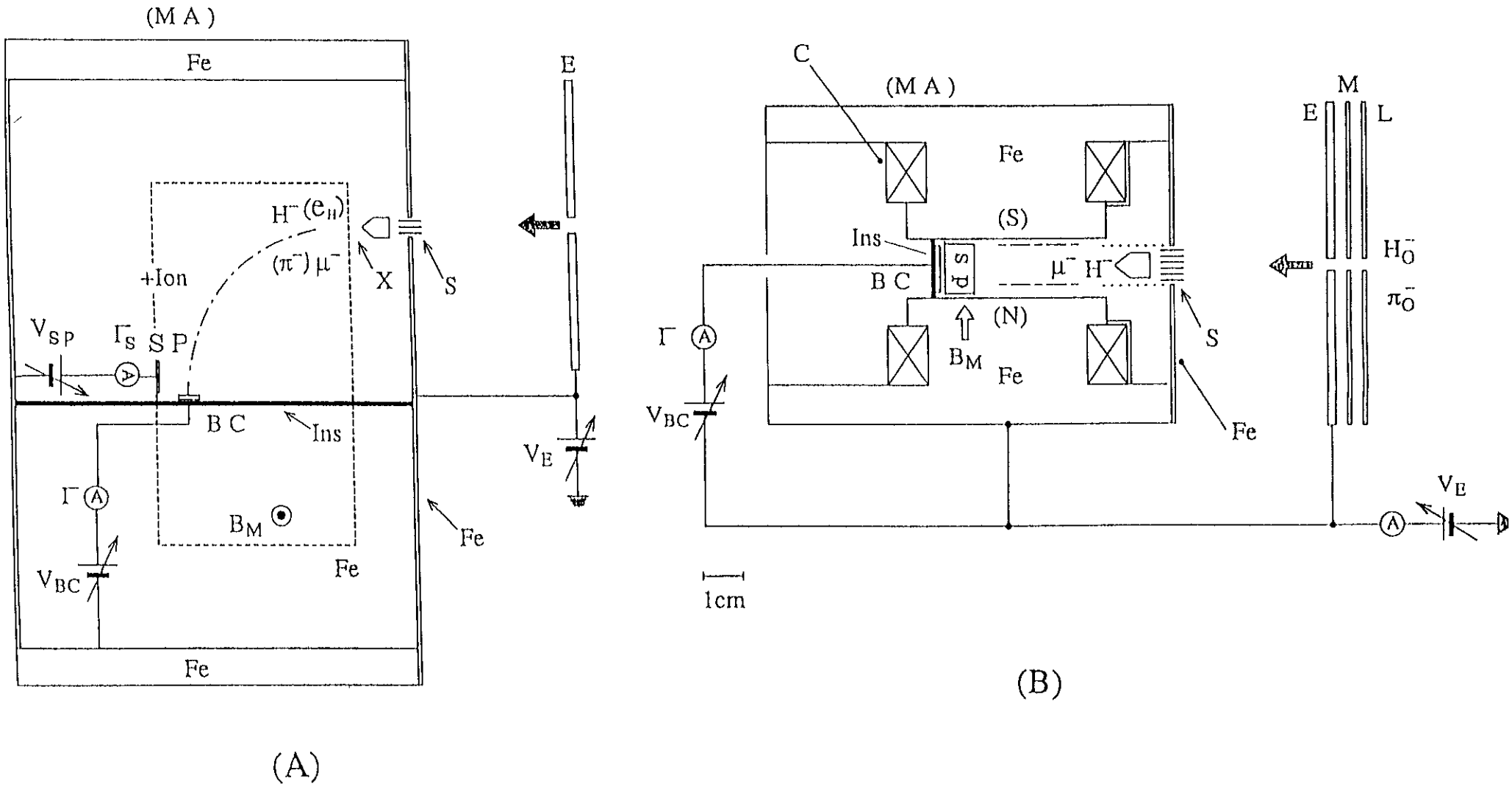
(M A)
Fe
E
$H^-(e_H)$
$(\pi^-)\ \mu^-$
+Ion
X
S
V_{SP}
Γ_S
S P
B C
Ins
V_E
Γ
A
B_M
Fe
V_{BC}
Fe
Fe
(A)
C
(M A)
Fe
(S)
Ins
B C
S P
μ^- H^-
(N)
B_M
Fe
S
Fe
Γ
A
V_{BC}
M
E
L
H_O^-
π_O^-
V_E
A
1cm
(B)

Fig. 2

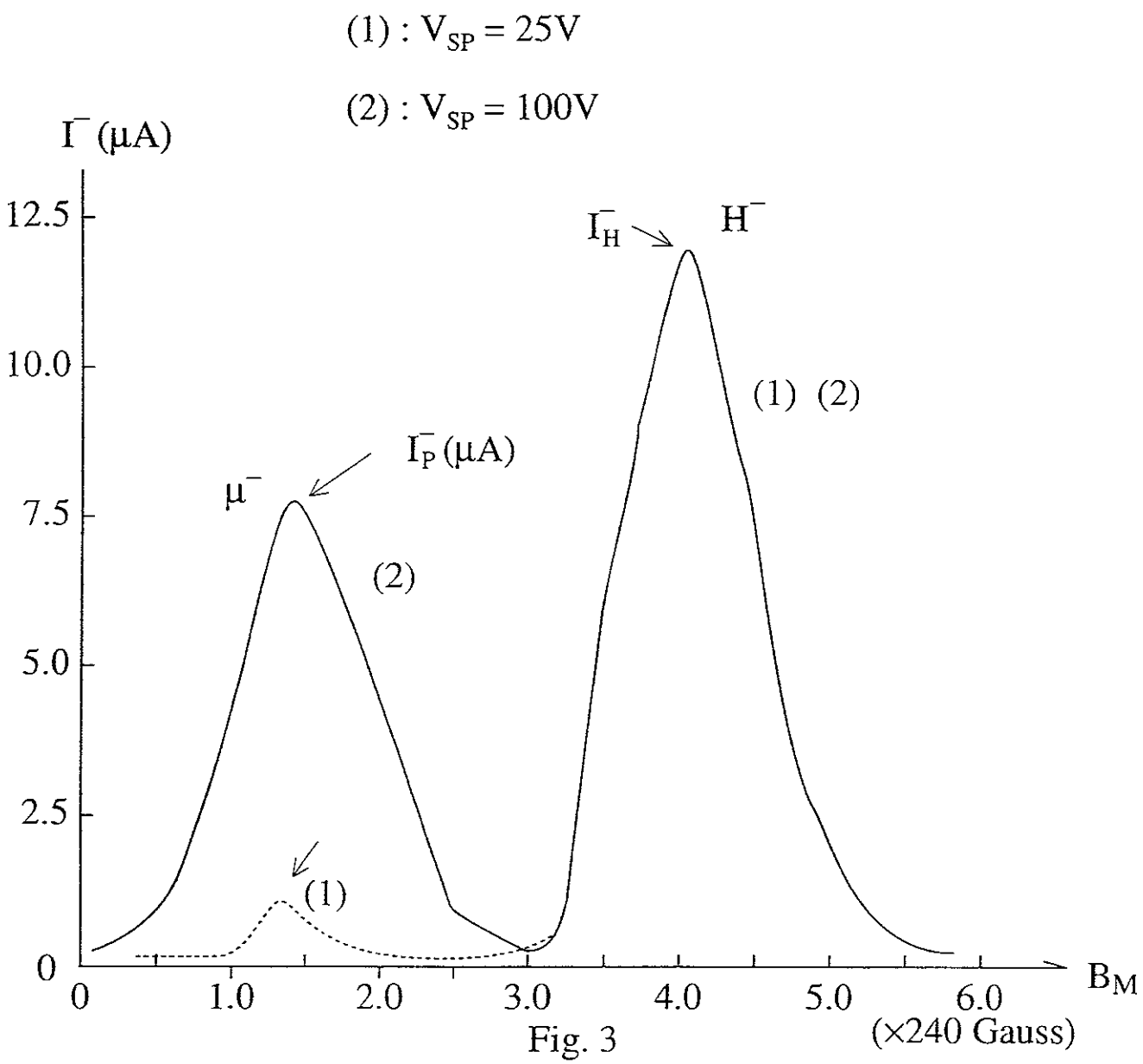
(1) : V_{SP} = 25V
(2) : V_{SP} = 100V
I^- (μA)
12.5
10.0
7.5
5.0
2.5
0
I^-_H
H^-
(1) (2)
I^-_P (μA)
μ^-
(2)
(1)
0
1.0
2.0
3.0
4.0
5.0
6.0
B_M
(×240 Gauss)

Fig. 3

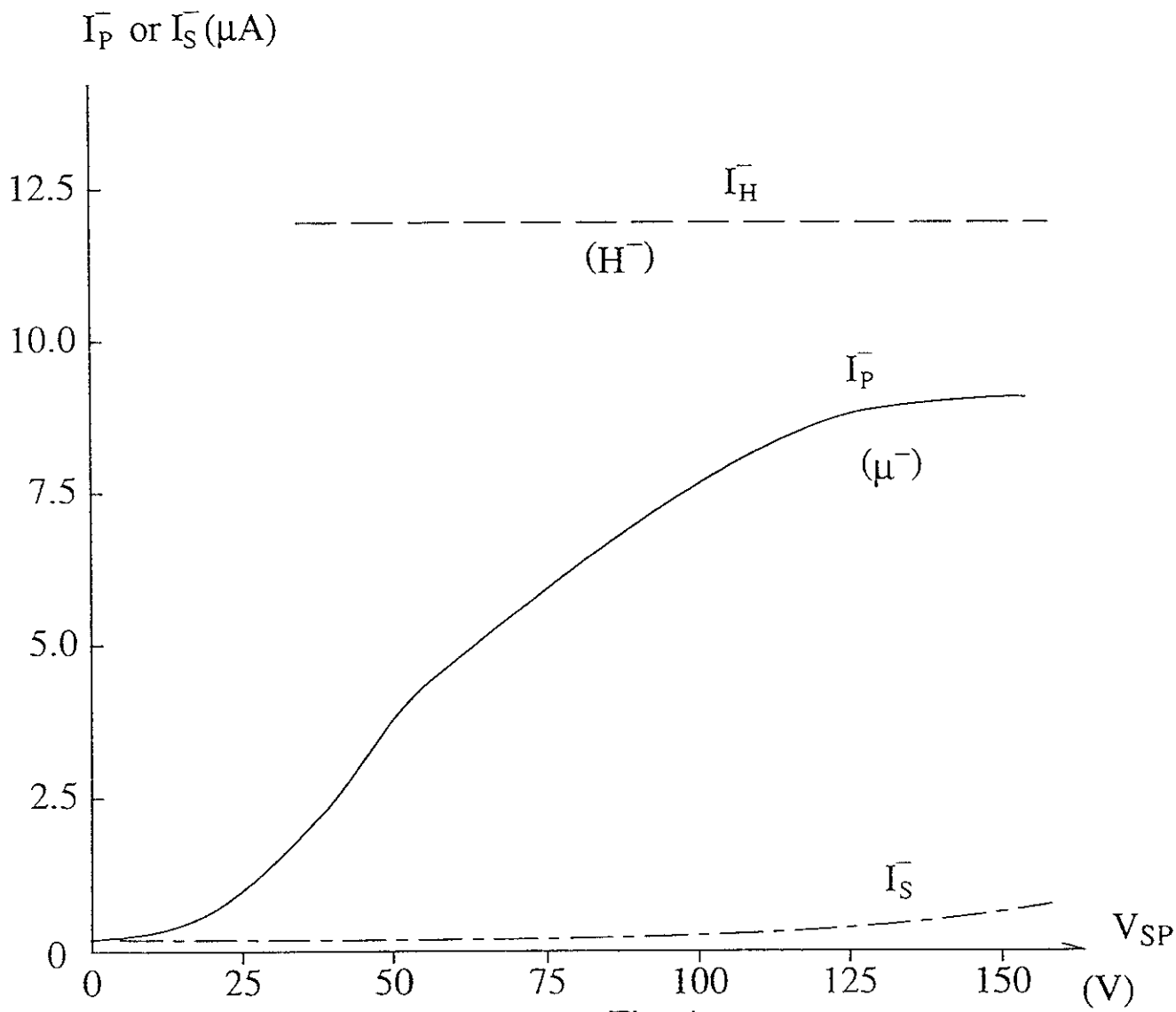
I_P^- or I_S^- (μA)
12.5
10.0
7.5
5.0
2.5
0
I_H^-
(H^-)
I_P^-
(μ^-)
I_S^-
V_{SP}
0
25
50
75
100
125
150
(V)

Fig. 4

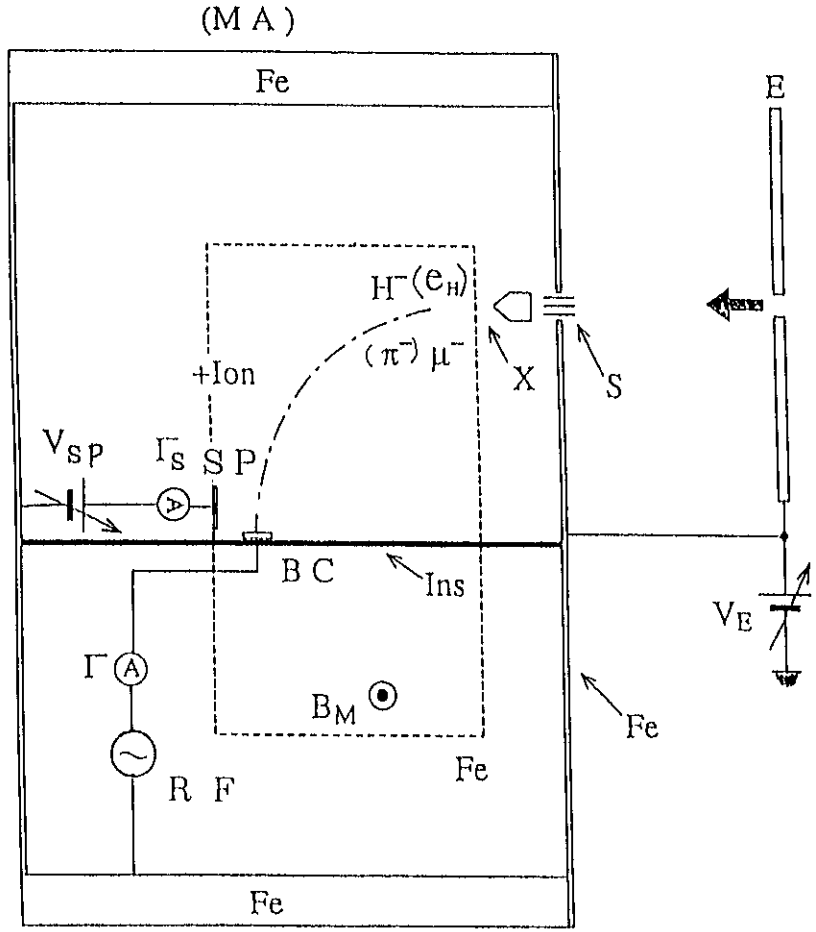
(M A)
Fe
E
H⁻(eH)
(π⁻) μ⁻
+Ion
X
S
VSP
Γ⁻S
S P
B C
Ins
VE
Γ
BM
Fe
R F
Fe
Fe

(A)

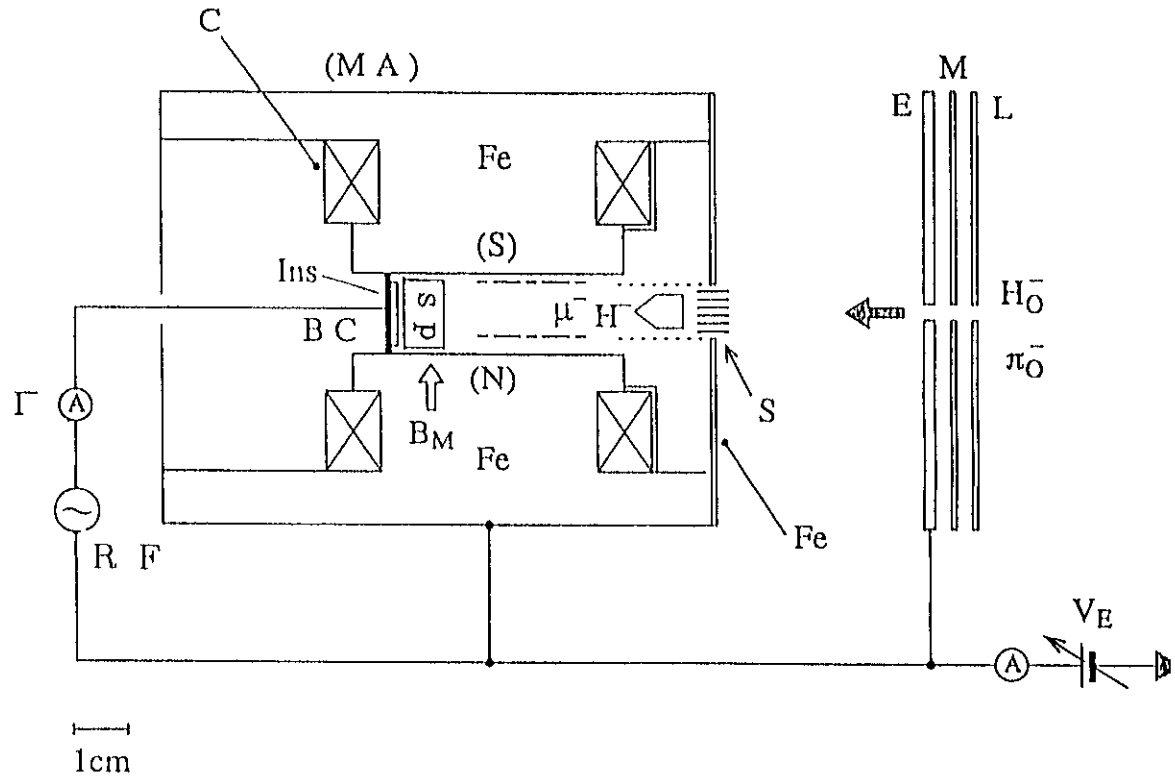
C
(M A)
Fe
(S)
Ins
B C
S P
μ⁻ H⁻
(N)
BM
Fe
S
Fe
R F
Γ
M
E
L
H⁻O
π⁻O
VE
1cm

(B)

Fig. 5

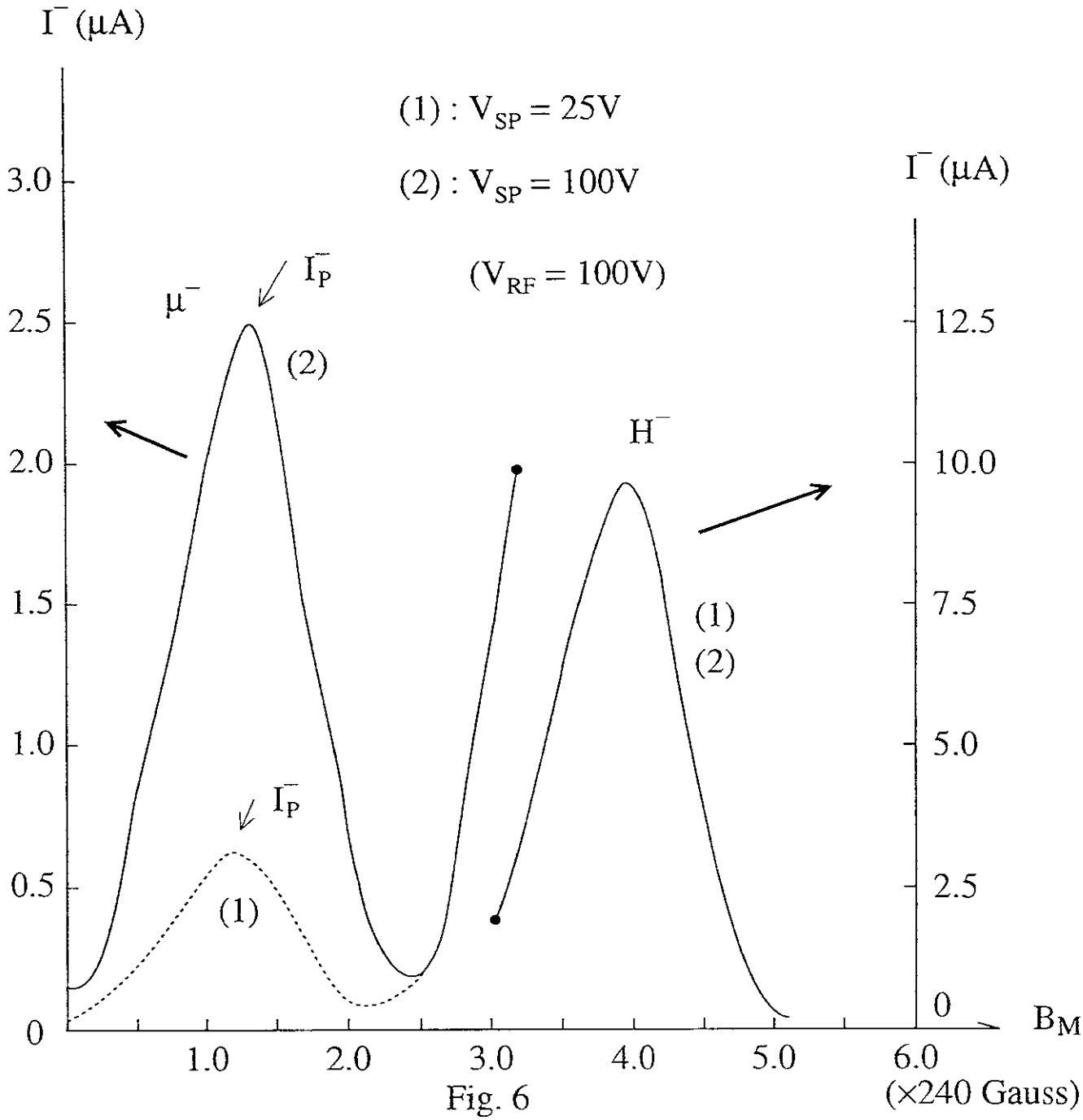
I⁻ (μA)
(1) : V_SP = 25V
(2) : V_SP = 100V
(V_RF = 100V)
I⁻ (μA)
3.0
2.5
2.0
1.5
1.0
0.5
0
μ⁻
I⁻P
(2)
H⁻
(1)
(2)
I⁻P
(1)
12.5
10.0
7.5
5.0
2.5
0
B_M
1.0
2.0
3.0
4.0
5.0
6.0
(×240 Gauss)

Fig. 6

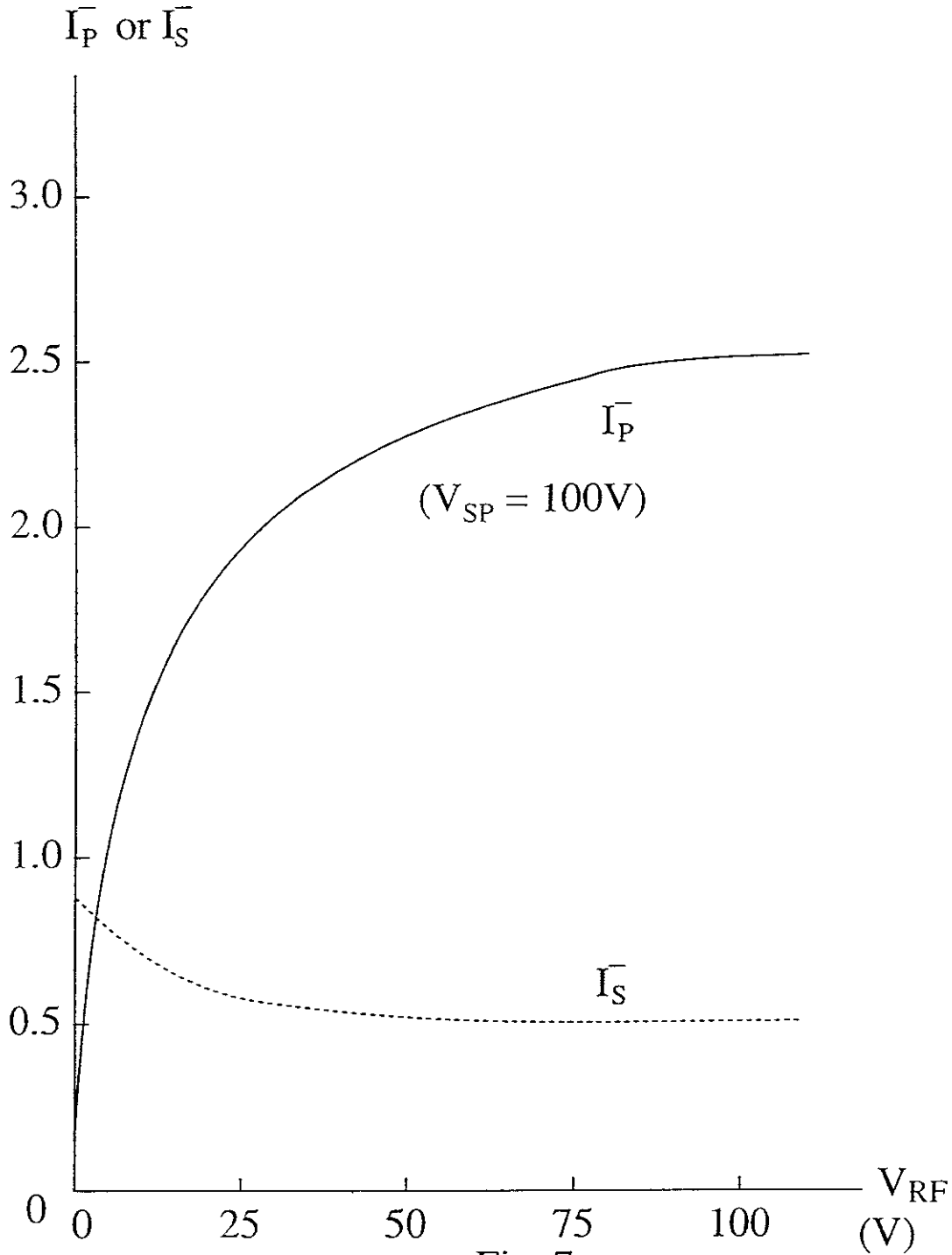
$\bar{I_P}$ or $\bar{I_S}$
3.0
2.5
2.0
1.5
1.0
0.5
0
$\bar{I_P}$
(V_{SP} = 100V)
$\bar{I_S}$
0
25
50
75
100
V_{RF}
(V)
Fig. 7

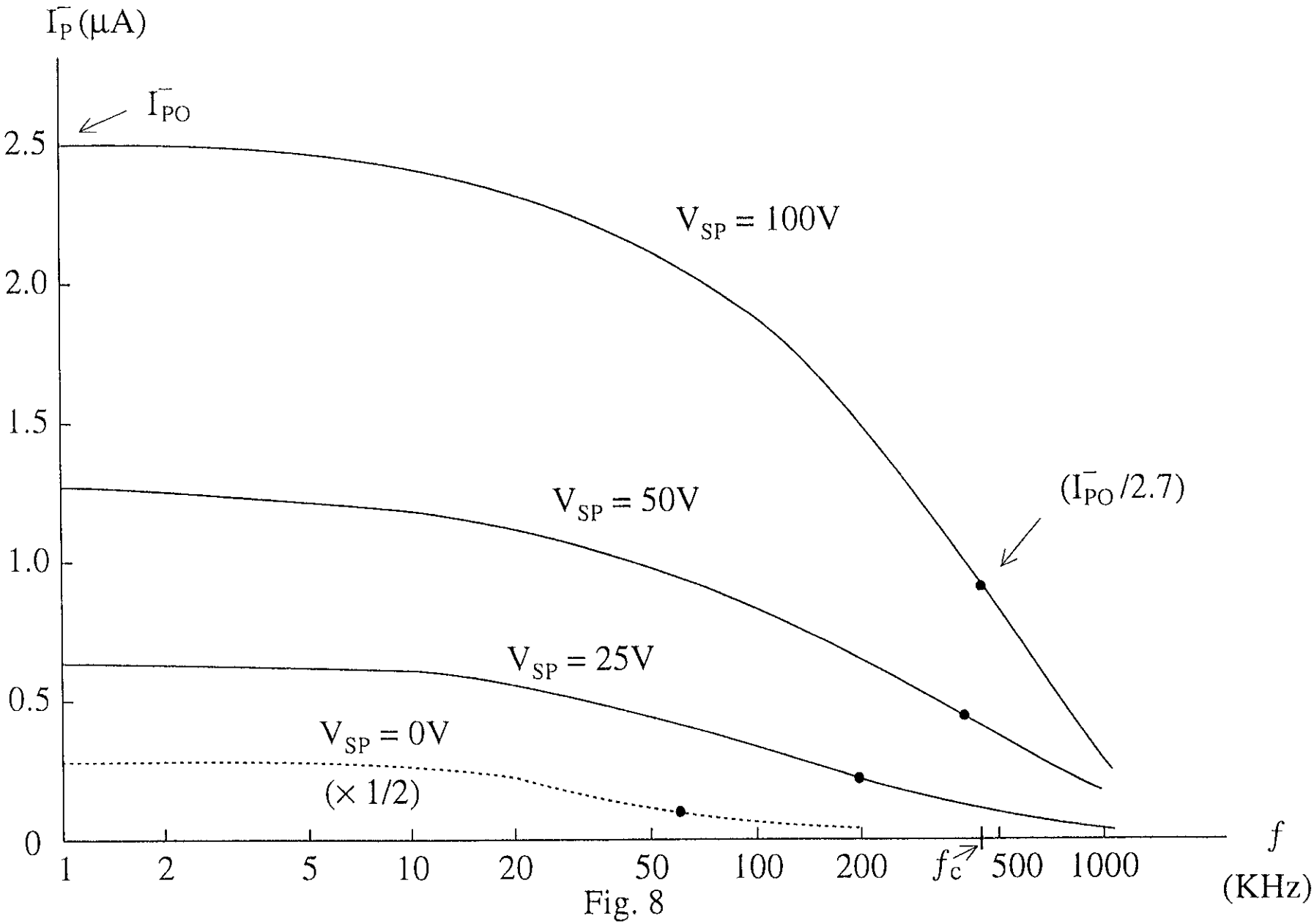
$\bar{I}_P$ (μA)
$\bar{I}_{PO}$
2.5
2.0
1.5
1.0
0.5
0
V_{SP} = 100V
V_{SP} = 50V
V_{SP} = 25V
V_{SP} = 0V
(× 1/2)
($\bar{I}_{PO}$/2.7)
1
2
5
10
20
50
100
200
f_c
500
1000
f
(KHz)

Fig. 8

Recent Issues of NIFS Series

NIFS-491 A Ejiri, K Shinohara and K Kawahata
An Algorithm to Remove Fringe Jumps and its Application to Microwave Reflectometry, Apr 1997

NIFS-492 K Ichiguchi, N Nakajima, M Okamoto
Bootstrap Current in the Large Helical Device with Unbalanced Helical Coil Currents, Apr 1997

NIFS-493 S Ishiguro, T Sato, H Takamaru and The Complexity Simulation Group,
V-shaped dc Potential Structure Caused by Current-driven Electrostatic Ion-cyclotron Instability, May 1997

NIFS-494 K Nishimura, R Horiuchi, T Sato,
Tilt Stabilization by Energetic Ions Crossing Magnetic Separatrix in Field-Reversed Configuration, June 1997

NIFS-495 T -H Watanabe and T Sato,
Magnetohydrodynamic Approach to the Feedback Instability, July 1997

NIFS-496 K Itoh, T Ohkawa, S -I Itoh, M Yagi and A. Fukuyama
Suppression of Plasma Turbulence by Asymmetric Superthermal Ions, July 1997

NIFS-497 T. Takahashi, Y Tomita, H Momota and Nikita V Shabrov,
Collisionless Pitch Angle Scattering of Plasma Ions at the Edge Region of an FRC, July 1997

NIFS-498 M Tanaka, A Yu Grosberg, V S Pande and T Tanaka,
Molecular Dynamics and Structure Organization in Strongly-Coupled Chain of Charged Particles July 1997

NIFS-499 S. Goto and S Kida,
Direct-interaction Approximation and Reynolds-number Reversed Expansion for a Dynamical System, July 1997

NIFS-500 K Tsuzuki, N Inoue, A Sagara, N Noda, O. Motojima, T Mochizuki, T Hino and T. Yamashina,
Dynamic Behavior of Hydrogen Atoms with a Boronized Wall, July 1997

NIFS-501 I Viniar and S Sudo,
Multibarrel Repetitive Injector with a Porous Pellet Formation Unit; July 1997

NIFS-502 V Vdovin, T Watari and A Fukuyama
An Option of ICRF Ion Heating Scenario in Large Helical Device, July 1997

NIFS-503 E Segre and S Kida,
Late States of Incompressible 2D Decaying Vorticity Fields, Aug 1997

NIFS-504 S Fujiwara and T Sato
Molecular Dynamics Simulation of Structural Formation of Short Polymer Chains, Aug 1997

NIFS-505 S. Bazdenkov and T Sato
Low-Dimensional Model of Resistive Interchange Convection in Magnetized Plasmas Sep. 1997

NIFS-506 H Kitauchi and S Kida,
Intensification of Magnetic Field by Concentrate-and-Stretch of Magnetic Flux Lines Sep 1997

NIFS-507 R L Dewar,
Reduced form of MHD Lagrangian for Ballooning Modes, Sep. 1997

NIFS-508 Y -N Nejoh
Dynamics of the Dust Charging on Electrostatic Waves in a Dusty Plasma with Trapped Electrons, Sep 1997

NIFS-509 E Matsunaga, T Yabe and M. Tajima,
Baroclinic Vortex Generation by a Comet Shoemaker-Levy 9 Impact, Sep 1997

NIFS-510 C C Hegna and N Nakajima,
On the Stability of Mercier and Ballooning Modes in Stellarator Configurations Oct 1997

NIFS-511 K. Orito and T Hatori,
Rotation and Oscillation of Nonlinear Dipole Vortex in the Drift-Unstable Plasma Oct 1997

NIFS-512 J Uramoto,
Clear Detection of Negative Pionlike Particles from H_2 Gas Discharge in Magnetic Field Oct 1997

NIFS-513 T. Shimozuma, M Sato, Y. Takita, S. Ito, S. Kubo, H. Idei, K Ohkubo T. Watari, T S Chu, K. Felch, P Cahalan and C.M. Loring, Jr,
The First Preliminary Experiments on an 84 GHz Gyrotron with a Single-Stage Depressed Collector, Oct. 1997

NIFS-514 T. Shimozuma, S Morimoto, M. Sato, Y Takita, S. Ito, S. Kubo, H. Idei, K. Ohkubo and T. Watari,
A Forced Gas-Cooled Single-Disk Window Using Silicon Nitride Composite for High Power CW Millimeter Waves; Oct 1997

NIFS-515 K. Akaishi,
On the Solution of the Outgassing Equation for the Pump-down of an Unbaked Vacuum System, Oct. 1997

NIFS-516 *Papers Presented at the 6th H-mode Workshop (Seeon, Germany)*: Oct 1997

NIFS-517 John L. Johnson,
The Quest for Fusion Energy, Oct. 1997

NIFS-518 J. Chen, N. Nakajima and M. Okamoto,
Shift-and-Inverse Lanczos Algorithm for Ideal MHD Stability Analysis; Nov. 1997

NIFS-519 M. Yokoyama N Nakajima and M Okamoto,
Nonlinear Incompressible Poloidal Viscosity in L=2 Heliotron and Quasi-Symmetric Stellarators; Nov. 1997

NIFS-520 S Kida and H Miura
Identificaiton and Analysis of Vortical Structures Nov 1997

NIFS-521 K. Ida, S Nishimura, T Minami, K Tanaka, S. Okamura, M Osakabe, H. Idei, S Kubo, C Takahashi and K Matsuoka,
High Ion Temperature Mode in CHS Heliotron/torsatron Plasmas; Nov 1997

NIFS-522 M. Yokoyama, N. Nakajima and M Okamoto,
Realization and Classification of Symmetric Stellarator Configurations through Plasma Boundary Modulations: Dec. 1997

NIFS-523 H. Kitauchi,
Topological Structure of Magnetic Flux Lines Generated by Thermal Convection in a Rotating Spherical Shell; Dec. 1997

NIFS-524 T. Ohkawa,
Tunneling Electron Trap, Dec 1997

NIFS-525 K. Itoh, S.-I. Itoh, M Yagi, A Fukuyama,
Solitary Radial Electric Field Structure in Tokamak Plasmas Dec 1997

NIFS-526 Andrey N Lyakhov,
Alfven Instabilities in FRC Plasma; Dec 1997

NIFS-527 J Uramoto
Net Current Increment of negative Muonlike Particle Produced by the Electron and Positive Ion Bunch-method: Dec 1997

NIFS-528 Andrey N Lyakhov,
Comments on Electrostastic Drift Instabilities in Field Reversed Configuraiton, Dec. 1997

NIFS-529 J. Uramoto,
Pair Creation of Negative and Positive Pionlike (Muonlike) Particle by Interaction between an Electron Bunch and a Positive Ion Bunch: Dec. 1997

NIFS-530 J. Uramoto,
Measuring Method of Decay Time of Negative Muonlike Particle by Beam Collector Applied RF Bias Voltage; Dec. 1997